DOI: https://doi.org/10.4038/sljp.v26i2.8159

INSTITUTE OF PHYSICS – SRI LANKA

Research Article

Structural, electronic, vibrational and superconducting properties of LiFeP pnictide superconductor - An Ab-initio approach

Aditya M. Vora*

Department of Physics, University School of Sciences, Gujarat University, Navrangpura, Ahmedabad 380 009, Gujarat, India

Abstract

Using the generalised gradient approximation (GGA) and an ultrasoft pseudopotential, we report on the structural, electrical, vibrational, and superconducting properties of LiFeP, an iron pnictide superconductor. The 3s state of P is regulated in the region considerably below the Fermi level, the 3s state of Li is above the Fermi level, and the 3d state of Fe is close to the Fermi level. The underlying bands close to the Fermi level reveal the metallic character of LiFeP. The positive frequencies of the phonon dispersion curves confirm the material's dynamical stability. A weak electron-phonon coupling (EPC), a measure of decreased electron scattering, indicates poor superconductivity in the material being studied. However, the big difference between the calculated T_C results and the experimental data shows that to improve T_C, the electron-phonon interaction needs to be 2.5–3.0 times stronger. Moreover, weak electron-phonon coupling is indicated by the effective interaction strength (N_0V) values and show superconducting nature.

Keywords: Ultrasoft pseudopotential, Iron pnictide superconductors, Density functional theory (DFT), Generalized gradient approximation (GGA), Structural Properties, Electronic Properties, Vibrational Properties, Superconductors

* Corresponding author: voraam@gmail.com

1. INTRODUCTION

A range of multilayer FeAs superconductors have been created by researchers in the field since the discovery of superconductivity in $LaFeAsO_{1-x}F_x$ at T_C 26 K [1, 2]. Materials belonging to the FeAs family have been demonstrated to be more active than cuprates due to their fragility [3-5]. Designing the cuprates in a desired structure is likewise a challenging procedure. On the other hand, research on NaFeAs and LiFeAs–Fe pnictide superconductors (FePSC) has been reported by Dai *et al.* [2]. According to Shein and Ivanovskii [6], the first principle hypothesis has been used to compare the electrical properties of LiFeP with LiFeAs.

A major breakthrough in condensed matter physics was made in 2008 with the discovery of Fe-based pnictide superconductors, which are binary mixtures of the V-group elements N, P, As, Sb, and Bi. In the past decade, both theoretical and experimental condensed matter researchers have focused a great deal of emphasis on the standard state properties of such materials, including their magnetism, pairing mechanism, symmetry, and pairing gap structure [4].

Jelena [7] used ab initio methods to investigate superconductivity in graphene and related materials, including doped graphene and magnesium-diboride monolayer. Multicomponent superconductivity in bulk to atomically thin materials has been described by Bekaert [8]. Superconducting materials, which display an amazing physical state of matter, have advanced rapidly, with a single coherent quantum state spanning metres or even kilometres [7-11]. Understanding this phenomenon and having a variety of materials with unique properties are essential for the successful use of superconductors [7-11]. A comprehensive analysis of theoretical and experimental research on Fe-based superconductors is published in [11]. The stability, electrical, and optical characteristics of 2D $M_2Si_2N_4$ materials have been studied systematically by Ding and colleagues using first-principles computations [12]. Romanin [13] investigated electron-phonon interactions in low-dimensional carbon allotropes, and Talantsev [14] proposed a classification scheme for nonadiabatic effects in superconductors. While, Kanoun and associates [15] theoretically evaluate the electronic structures and phonon dispersion of Ce_2XN_2 (X = S, Se, and Te) ternary compounds using first-principles calculations.

Numerous Fe-pnictides are part of the large family of FePSC, including '1111' systems like RFeAsO, where 'R' is the rare earth element; '122' systems like XFe2As2, where X is an alkaline earth metal; '111' systems like LiFeAs; and Fe-chalcogenides, which are Fe-based

compounds made from the various elements of the XVI group of the periodic table, i.e., S, Se, and Te, such as $FeTe_{1-x}Se_x$ and AFe_2, where A is a K, Rb, or Cs atom [16].

The parental complexes of Fe-based pnictide superconductors are frequently metals, in contrast to cuprate superconductors, which have parent compounds that are antiferromagnetically ordered Mott insulators [1-5]. Pressure, isovalent substitution of one pnictide element for another (for example, As for P), or both can result in superconductivity (SC) in FePSCs. Consequently, in LaFePO and LiFeAs systems, the SC instead of a magnetic order appears at zero doping [4, 5].

Superconducting current is related to a charge reservoir, which may be an alkaline earth metal like magnesium or an alkali metal like potassium, because pnictide compounds usually contain iron pnictide layers. Furthermore, it is asserted that the itinerant nature of SC in its normal form can help explain the phenomena of high-temperature SC in pnictide superconductors. A FeP layer with a structure similar to LiFeAs is present in LiFeP, a newly found iron pnictide superconductor. The first arsenic-free analogue of the '111' iron pnictides family with its transition temperature, around $T_C \sim 6$ K [1], makes it a low-temperature superconductor.

Along with pnictides and oxypnictides, iron chalcogenides also make it to the superconducting phase. The T_C of β-FeSe, a straightforward iron chalcogen superconductor, is 8 K at normal pressure and 36.7 K at high pressure, indicating that it is typically superconducting. The formation of FeSe single-layered films on doped $SrTiO_3$ substrates has also been observed to raise the critical temperature to 109 K [1, 2].

The discovery of superconductivity in LaFeAsO led to the discovery of numerous iron pnictide superconductors [16]. It's a member of the iron pnictide superconductor '1111' family. Two further iron pnictide superconductors that have been revealed are LiFeP and LiFeAs of the family '111'. The basic details of LiFeAs have been disclosed by Tapp *et al.* [16]. However, LiFeP was first synthesised in 2009 using the standard solid-state reaction method. The LiFeP has a P4/nmm space group and is tetragonal in form. Because Li atoms are joined to the FeP building blocks to form a multilayer structure, Li acts as the charge reservoir. The transition temperature T_C of LiFeP is around 6 K [6]. Furthermore, its lattice parameters have experimental values of a = b = 3.692 Å and c = 6.031 Å, respectively [4]. It is seen that the T_C drops under pressure at a rate of 1.38 K/GPa, leading to a lower transition temperature T_C, which is consistent with findings previously published in 2009 [4].

Together with the discovery of superconductivity in LaOFeP with T_C = 4 K, they were fundamentally discovered in 2006 by Kamihara and associates [17]. 2008 saw the discovery of La[$O_{1-x}F_x$]FeAs, a more recent iron pnictide superconductor with T_C = 26 K. Additionally, when 4 GPa of pressure is applied, it displays a superconducting nature at T_C = 43 K. The transition temperature (T_C) increases to 52 K when other rare earth elements are substituted for lanthanum [1]. Iron and pnictide layers are used to construct such superconductors. They also fall under the periodic table's group XV, which also contains elements like arsenic (As) and phosphorus (P). Because of this, it is composed of FeAs layers with alternating spacers or charge reservoir blocks composed of alkaline earth metals, such as potassium or magnesium. However, layers of iron in iron-based pnictide superconductors often contain oxypnictides instead of pnictides. Many researchers have expressed interest in such superconductors. Iron pnictide (oxypnictide) compounds frequently have tetragonal or orthorhombic structural phases. Furthermore, the transition temperature T_C varies in response to variations in the As-Fe-As bond angles [5].

The primary goal of this work is to evaluate LiFeP's superconducting properties by comprehending its electronic and phononic properties. The study sheds light on its poor electron-phonon coupling, dynamical stability, and metallic behaviour, all of which point to limited superconductivity. In order to improve superconductivity, stronger electron-phonon interactions are required, as demonstrated by the comparison of theoretical and experimental superconducting transition temperatures (TC). These discoveries advance our knowledge of the mechanics behind superconductivity in iron-based materials and could guide future research into the creation of higher-TC superconductors.

Density Functional Theory (DFT)-based simulations are currently believed to be more realistic for evaluating the physical properties of different materials [5, 18-22]. The current work intends to investigate the structural, electrical, vibrational, and superconducting properties of LiFeP iron pnictide superconductor in a DFT environment to gain a deeper understanding of the relevance of the superconductivity phenomena and its applicability in various fields.

2. COMPUTATIONAL METHODOLOGY

In the current study, we have examined the material's structural, electrical, vibrational, and superconducting characteristics using the Quantum Espresso (QE) code [23]. Because it encourages density inhomogeneity, the Generalised Gradient Approximation (GGA) with

the Perdew-Burke-Einzerhof (PBE) functional is used to study the exchange correlation effects [24]. Here, 80 Ry is the cutoff for kinetic energy, and 80 Ry is the cutoff for charge density. Integration over the Brillouin zone is achieved using a 8 × 8 × 8 k-point mesh. The ultrasoft pseudopotentials [25] of three distinct elements - Li, Fe, and P - are used in the current work.

3. STRUCTURAL PROPERTIES

Equilibrium geometry was produced by optimising the atomic locations of the structure. The structure was believed to have converged when the energy accuracy of 10^{-6} Ry was reached. The structure of the LiFeP in this case is tetragonal with space group P4/nmm. Li atoms surround its [Fe_2P_2] blocks, which alternate. The crystal structure of LiFeP is shown in **Figure 1**. The experimental values of the lattice parameters are a = b = 3.692 Å and c = 6.031 Å [4]. It is discovered that the optimised lattice parameter values, a = b = 3.707 Å and c = 6.167 Å, are in great agreement with the experimental values that are currently available [4]. Here, the primary symmetry points Γ→ Z → R → X → M → A are given a band structure.

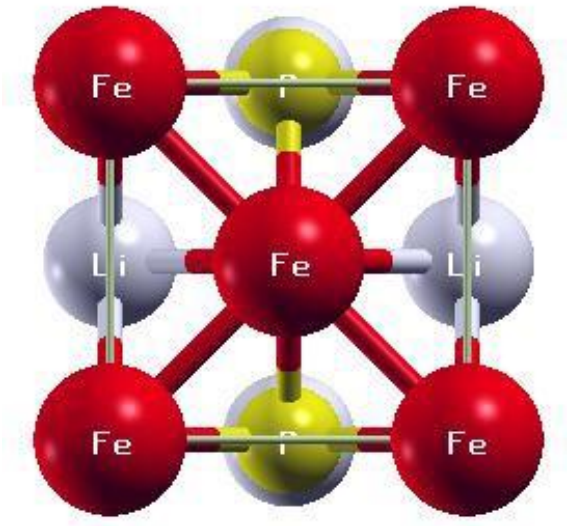

Figure 1. Crystal structures of LiFeP.

The unit cell of the material being studied consists of two Li, two Fe, and two P atoms, where the "Li" atoms are located in the (0, 1, 1) and (1, 0, 1) directions at (0.0, 0.5, 0.7) and (0.5, 0.0, 0.3), respectively. At coordinates (0.0, 0.0, 0.0) and (0.5, 0.5, 0.0), respectively, the 'Fe'

atoms are situated at the origin and in the (1, 1, 0) direction. Similarly, in the (1, 0, 1) and (0, 1, 1) orientations, the 'P' atoms are located at (0.5, 0.0, 0.8) and (0.0, 0.5, 0.2), respectively. The optimisation curves for the kinetic energy cutoff (Ecut), k-grid, and the ratio of the cell parameters (c/a) are shown in **Figures** 2(a-c), respectively. Initially, the lattice constants and atom positions are optimised using the Variable Cell Relaxation (vc-relax) technique. Later, the lattice parameter ratio (c/a) was tuned to validate the results. The GGA approach, which uses ultrasoft pseudopotentials as in QE code, is utilised to find the relaxed parameters [11]. The results of the predicted lattice parameter match the known experimental data [4] qualitatively, as **Table 1** illustrates. The percentage difference between the two findings is also explained in the same **Table 1**. The percentage difference between them is 1.4% and 5.5%, respectively.

Table 1. Calculated and experimental lattice parameters for LiFeP.

System	**Lattice constants (Å)**		**Deviation (%)**
	Calculated values	**Experimental values [4]**	
LiFeP	a = b = 3.706	a = b = 3.692	1.4
	-c = 5.849	c = -6.031	3.1
	c/a = 1.57835	c/a = 1.6335	5.5

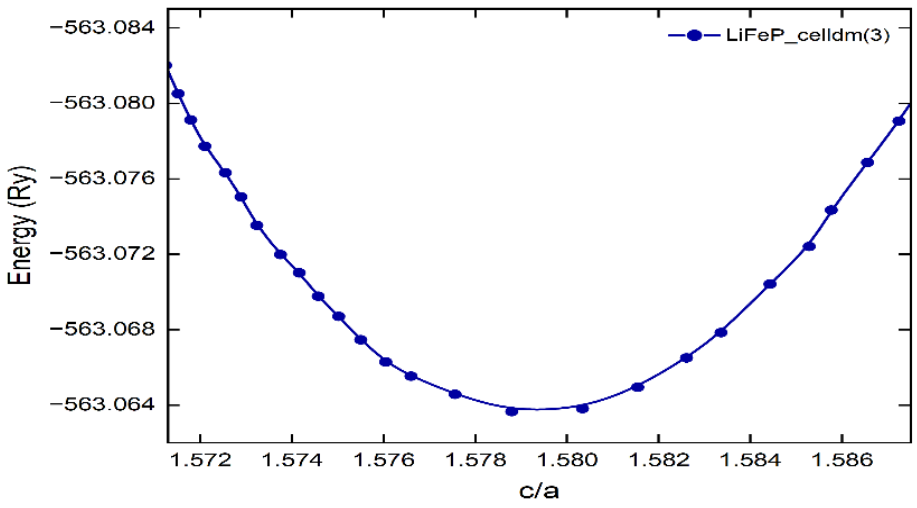

(a)

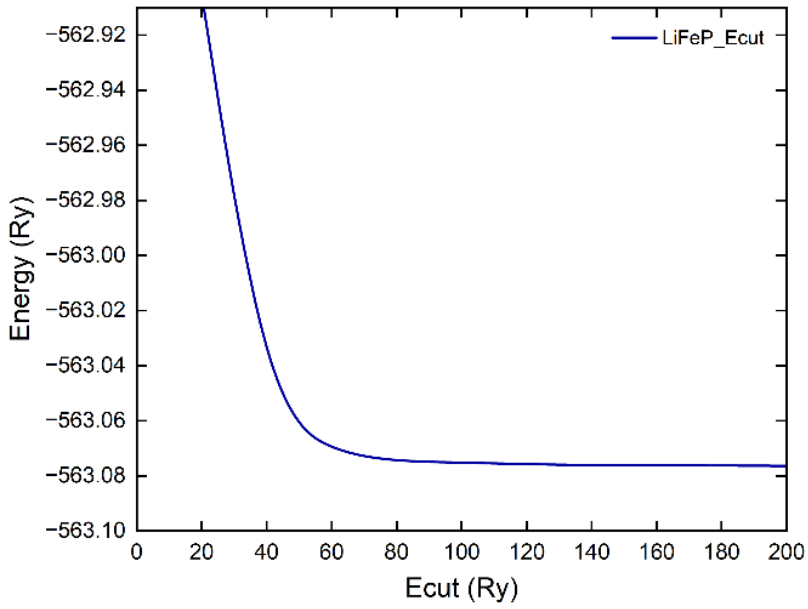

(b)

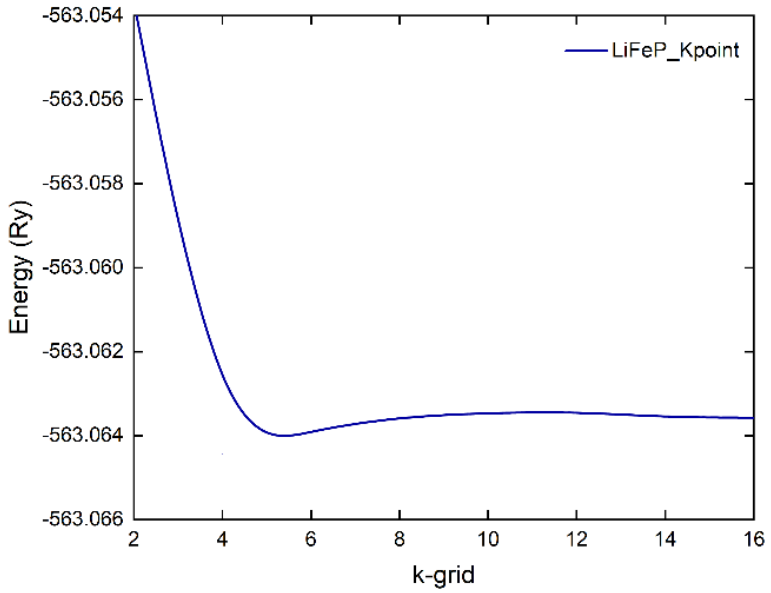

(c)

Figure 2. Optimization curves for (a) c/a, (b) E_{cut} and (c) k-grid for LiFeP.

4. ELECTRONIC PROPERTIES

The ground-state energy and electronic properties of the superconductor are estimated using the DFT. To understand the behaviour of the materials, estimates are made of the contributions of each element, electrons and holes, electronic band structure, electron DOS, PDOS, and Fermi surface topology [5, 18-22]. Since the materials are based on iron and exhibit ferromagnetic properties, the spin component is considered while doing the calculations for the electronic band structure and DOS in this instance [5, 18-22].

4.1. Band structure

Crystalline materials are described by their band structure, which shows how the material behaves in a two-dimensional representation of the energy of the crystal orbitals [26]. Because of their odd shapes and thin lines, "spaghetti diagrams" get their name [27]. The band structures across the high symmetry sites of the first Brillouin zone are shown using gnuplot [28] in **Figure 3**, respectively. In this instance, $\Gamma \rightarrow Z \rightarrow R \rightarrow X \rightarrow M \rightarrow A \rightarrow \Gamma$ is the name of the k-point path in reciprocal space. Both the 320 Ry charge density cutoff and the 80 Ry kinetic energy cutoff are applied. Monkhorst and Pack [29] advise sampling a 10×10×10 k-mesh. The computational work integrates over the Brillouin zone using a k-point mesh of 8×8×8.

In the band structure computations, a spin component is incorporated because of the naturally ferromagnetic element ‘Fe’. However, the studied material exhibits non-spin character. The two lowest bands in the aforementioned material's band diagram, which are located around -10.5 eV below the Fermi level (E_F), are primarily formed by P(3s) states (see peak in **Figure 4**). These bands are separated from near Fermi valence bands, which are located in the energy range of -5.8 eV to E_F and are primarily shaped by Fe(3d) and P(3p) states, by a gap of about 3.9 eV. The consistent TDOS in **Figure 4** includes these two main sub-bands. The conclusions of Shein and Ivanovski [6] are supported by this theoretical study.

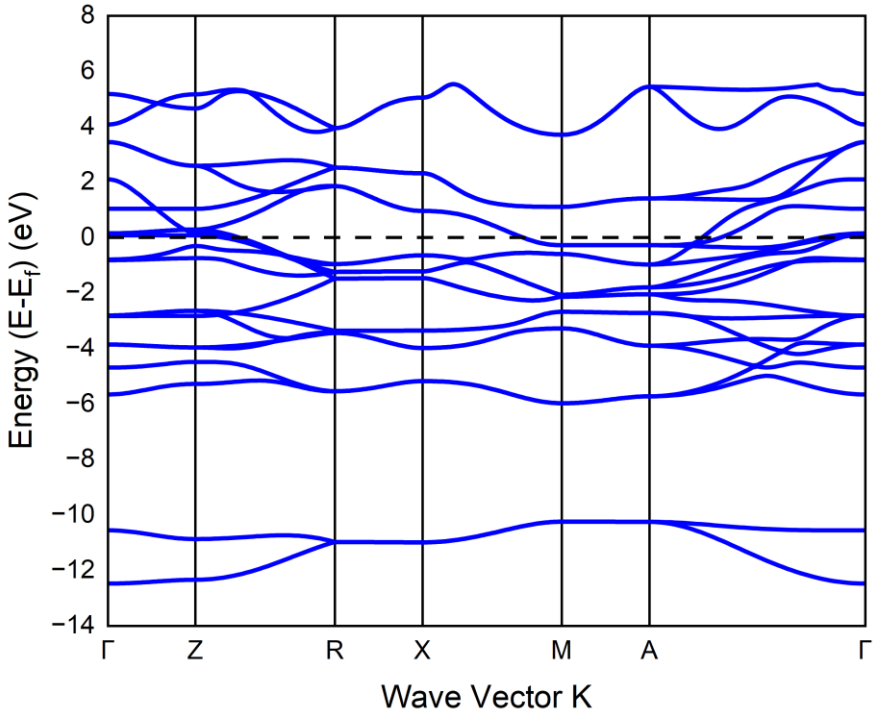

Figure 3. Electronic band structure of LiFeP.

4.2. Density of States (TDOS and PDOS)

In this case, the tetrahedral technique for integration over the Brillouin zone is used to get the density of states (DOS). **Figures 4** and **5** display the LiFeP pnictide superconductor's TDOS and PDOS, respectively. Deep below the Fermi zone, an electron density of about 1.7 states per eV is observed at -10 eV. At the Fermi level, there are 3.7 states of electrons per eV. **Figure 5** demonstrates that the band overlap at the Fermi energy (E_F) is mostly caused by the 3d orbital of Fe. Just below the E_F, at roughly -2.5 eV, quasi-core pnictogen bands are seen in the band structure because of the Fe_2P_2 blocks (**Figure 4**). The electron density is suppressed well below the E_F by the P's 3s orbital. In actuality, the orbital states of 'Li' contribute very little to the overall structure. The metallic aspect of the aforementioned superconductor is due to the presence of the 3d orbital of Fe and the Fe_2P_2 blocks, which produce pnictogen bands [5], revealing the nature of the electronic states responsible for superconductivity in the studied material. The diamagnetism of the LiFeP material may suggest that it is in the superconducting phase even if the highly ferromagnetic element Fe is present [5]. In BCS-type superconductivity, the TDOS, which is near to the Fermi energy (E_F), determines the Cooper pairing mechanism. However, LiFeP - pnictide superconductor has a moderate but non-zero TDOS, which is associated with the superconductivity. From the **Figure 4**, the PDOS decomposition can be used to identify specific atomic orbitals that

contribute to states near E_F. While, Fe (3d) orbitals dominate the DOS close to the Fermi level, P (3p) orbitals hybridise with Fe (3d) states to produce bonding and antibonding states. It is necessary to comprehend these contributions in order to describe electronic transport and superconducting pairing channels [6].

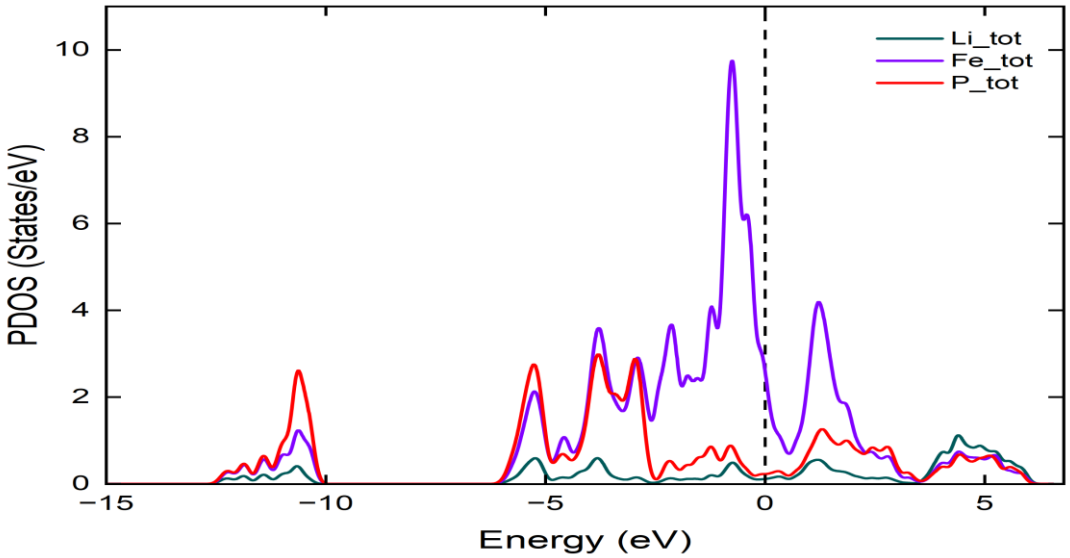

Figure 4. Total DOS of LiFeP.

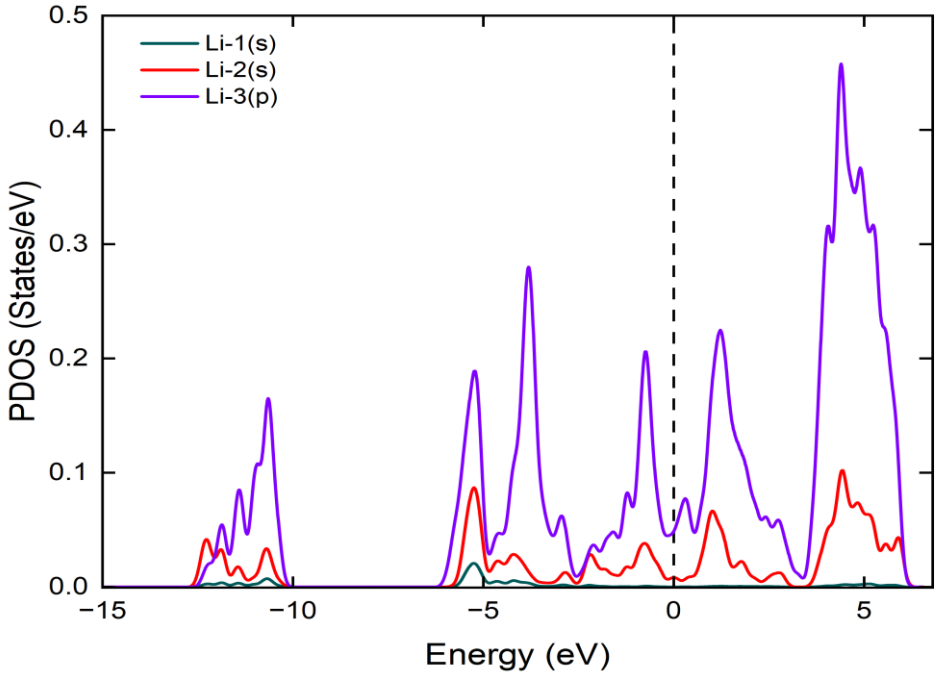

(a)

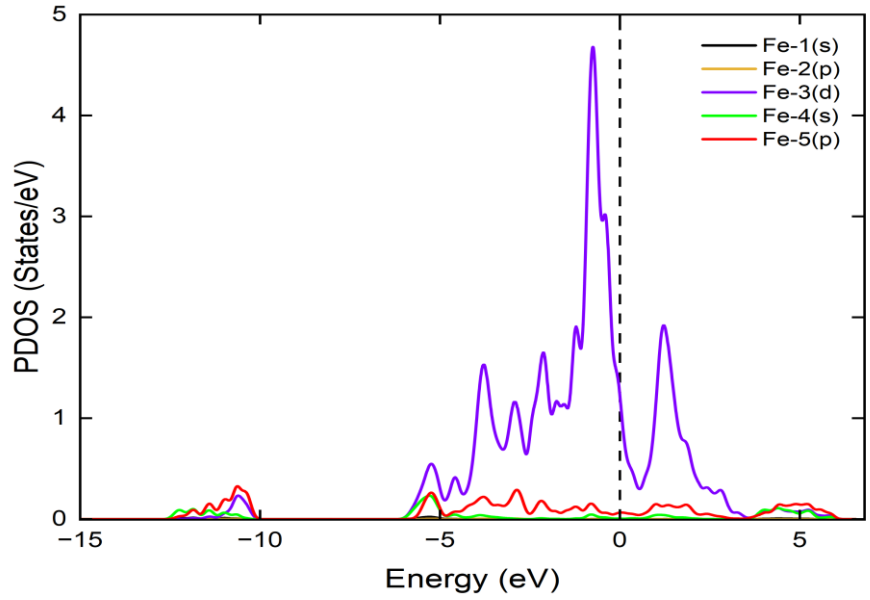

(b)

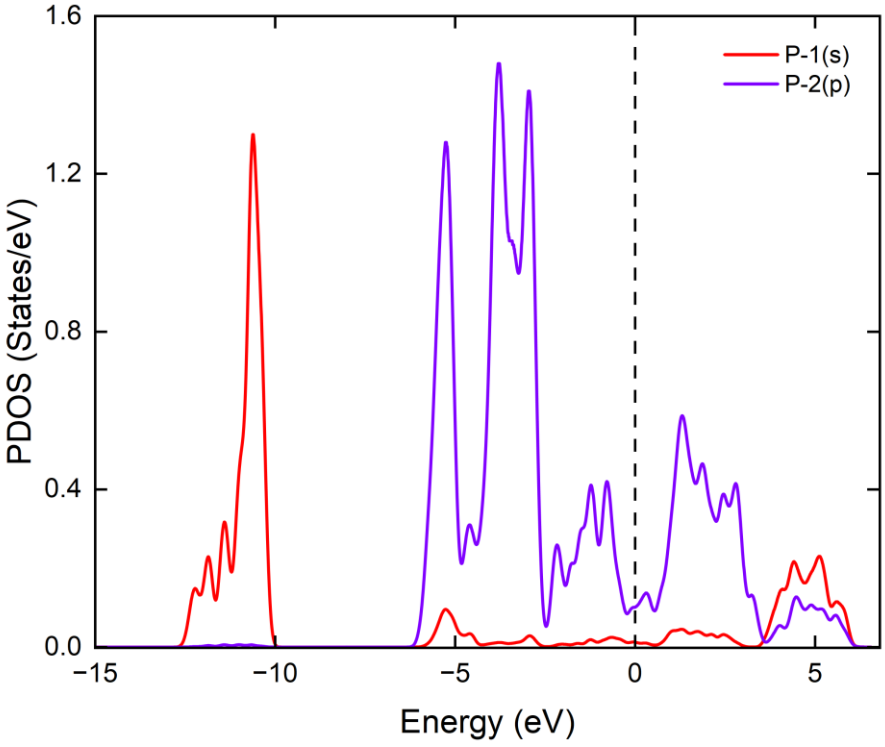

(c)

Figure 5. PDOS for LiFeP (a) Li, (b) Fe and (c) P.

4.3. The Fermi surfaces

In general, the idea that assists in the geometric representation of the relative occupation of the permitted unoccupied lattice bands in k-space is the Fermi surface [30]. Over the whole Fermi surface, the momentum space contains a continuous Fermi energy E_F. Analysing the

Fermi surface topology is essential for measuring the materials' electrical characteristics. Since the band structure and DOS for the spin-up and spin-down scenarios do not differ, the spin component is not included in the Fermi surface calculation. The Fermi surfaces are visualized using the XCrySDen [31]. The Fermi surfaces for aforementioned superconductor are shown in **Figure 6**. **Figure 4** of the band structure shows that there are five bands that span the Fermi energy (E_F) level. The matching Fermi surfaces of the five bands are displayed. They display the characteristic 2D nature of 'FeAs' superconductors, according to Sadovskii [32]. Fermi surfaces for a number of bands that cross the E_F are shown in **Figures 6(a)–(e)**. The Fermi surfaces for mixed bands are displayed in **Figures 6(f)** and **6(g)**. The hole-like concentric cylinders at the zone centre (Γ) and quasi-cylinders at the corners of the Brillouin zone in the M-A direction supply the electron contribution. Consequently, the occupied and unoccupied states are distinguished in the visualisation of the Fermi surfaces. Thus, a key determinant of the sensitivity of bonding-antibonding splitting would be the distance between the iron-pnictogen atoms in the covalent bonds [5]. Like FeAs superconductors, presently computed LiFeP's Fermi surfaces have a two-dimensional character reported in the literature [33-35]. It is made up of a set of sheets that run parallel to the K_Z direction. LiFeP, a tetragonal P4/nmm structure, crystallizes in a quasi-two-dimensional (2D) structure resulting from the layered nature of the Fe–P plane. The Fermi surface topology consists of multiple cylindrical sheets, originating from Fe (3d) orbitals. The multiband nature of the Fermi surface leads to complex superconducting pairing scenarios. LiFeP shows reduced density of states (DOS) at E_F, smaller hole pockets, and weaker electron correlations, suggesting weaker electron-phonon coupling and less favorable nesting. Experimental studies using the de Haas–van Alphen effect confirm the presence of multiple Fermi surface sheets in LiFeP and validate DFT predictions, confirming the low-energy electronic structure of the system [36-40].

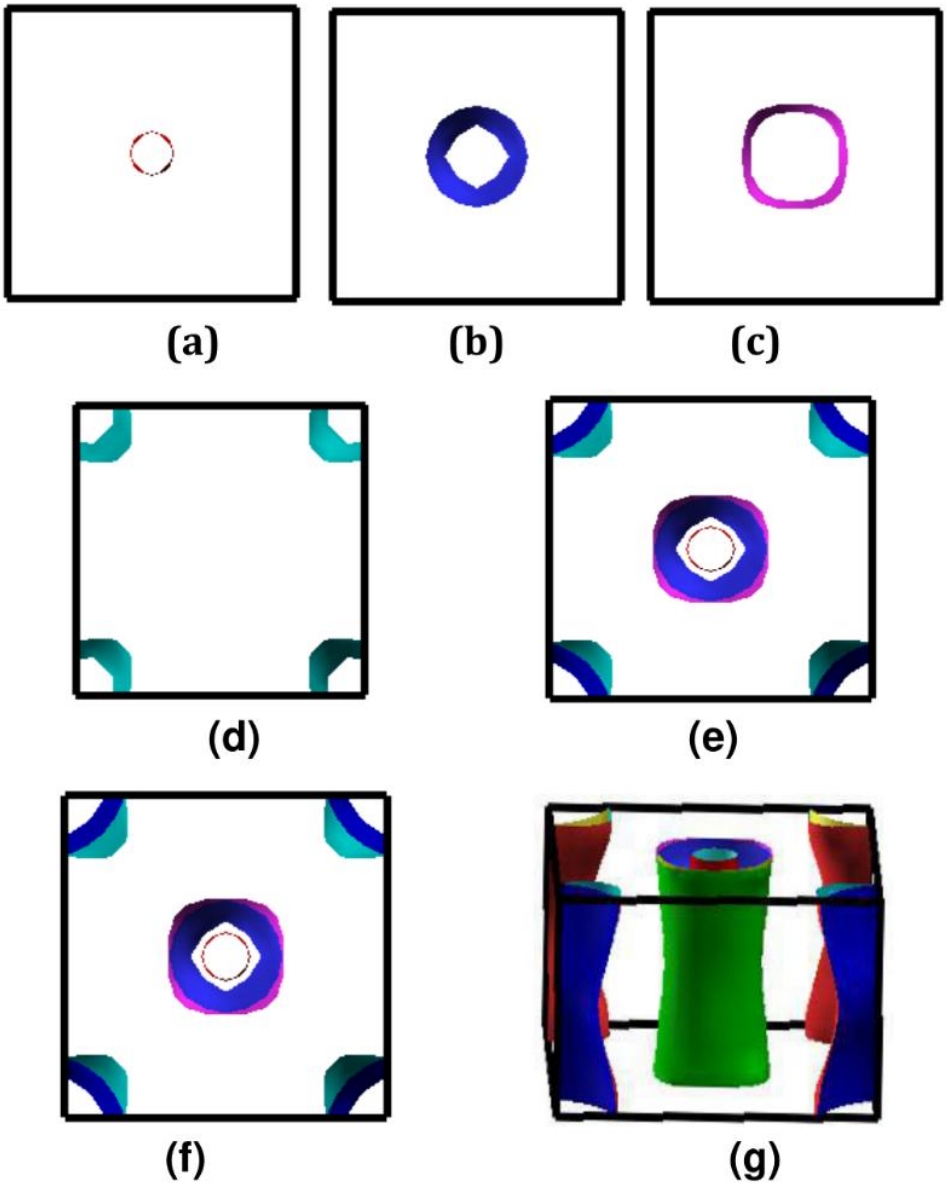

Figure 6. The Fermi surfaces of LiFeP for different bands (a)-(e) and for merged bands (f) and (g).

5. VIBRATIONAL PROPERTIES

5.1. Phonon Dispersion Curve

Phonons of stated materials are calculated using the "PHonon" package of the Quantum ESPRESSO algorithm [23]. Based on the Density Functional Perturbation Theory (DFPT), this package includes computational methods. The material's IR (infrared) and Raman spectra [23], effective charges, dielectric properties, electron-phonon coupling, and interatomic force constants can all be studied with it. For the plane wave basis, the phonon dispersion is calculated using the charge density cutoff of 400 and the kinetic energy cutoff

of 100 Ry. A k-mesh of 10×x10×x10 is employed, per Monkhorst-Pack [29]. We estimate the phonon dispersion over high symmetry sites of the Brillouin zone Γ→Z→R→Γ with a q-grid of 2×2×2.

The phonon dispersion curve and phonon density of states for LiFeP materials are shown in **Figures 7(a)** and **7(b)**. The unit cell, however, is made up of six atoms. As a result, there are 18 branches on the phonon dispersion curve. These eighteen branches reach non-zero frequency close to the gamma point, with three corresponding to the acoustic mode and fifteen to the optical mode. 421 cm^{-1} is the highest estimated phonon frequency. The dispersion curve contains five longitudinal optical branches (LO), one longitudinal acoustic branch (LA), two transverse acoustic branches (TA), and ten transverse optical branches (TO). The Γ-Z region still has a TA branch that is in poor condition. They frequently continue non-dispersively in the Γ-Z-R-X directions. It is clear from **Figure 7(a)** that the dispersion curve only includes positive frequencies, indicating the dynamic stability of the material under study. The phonon DOS exhibits some notable peaks are primarily caused by the optical branches' flat curve. Here, widely separated acoustic branches, particularly in the Fe–P layers and close to the Γ-point, indicate strong bonding interactions. The mechanical rigidity of these layers is essential for their electrical and superconducting properties and promotes strong carrier mobility and lattice stability. Compared to LiFeAs pnictide superconductors, LiFeP materials often show harder phonon modes, less pronounced softening, and lower electron-phonon coupling constants. This supports the idea that spin or orbital fluctuations, rather than phonon-mediated processes, are the source of superconductivity in LiFeP. Hence, LiFeP pnictide superconductors exhibit a wide phonon density of states, primarily due to electron-phonon interaction, particularly optical phonon modes, which are believed to be the main process causing the superconductivity. In conclusion, although we found that the P atoms are also disconnected from the Fe plane in certain modes, the Li seems to be mostly separated from the iron pnictogen plane [1]. Here, one can see imaginary frequencies seen in the phonon density of states curves between 200-300 cm^{-1} frequency range. It may be due to the crystallization of LiFeP in a tetragonal form. Dynamic instability at 0 K may be indicated by imaginary phonon modes in PDOS under certain circumstances. These modes might point to a lower-symmetry deformed phase that is connected to superconductivity. The Fe-P layer of the structure plays a major role in determining its electrical and vibrational properties. It is necessary to comprehend the effects

of the pairing mechanism on the electrical and lattice structures in unconventional superconductivity. It is required to perform convergence tests and recalculate phonons. [45].

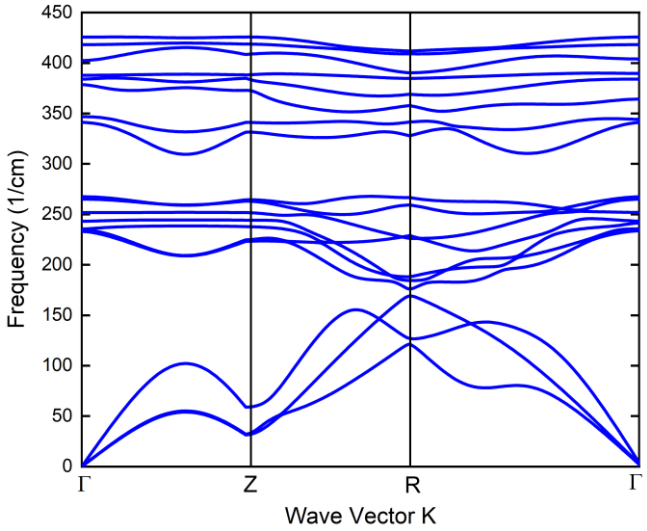

(a)

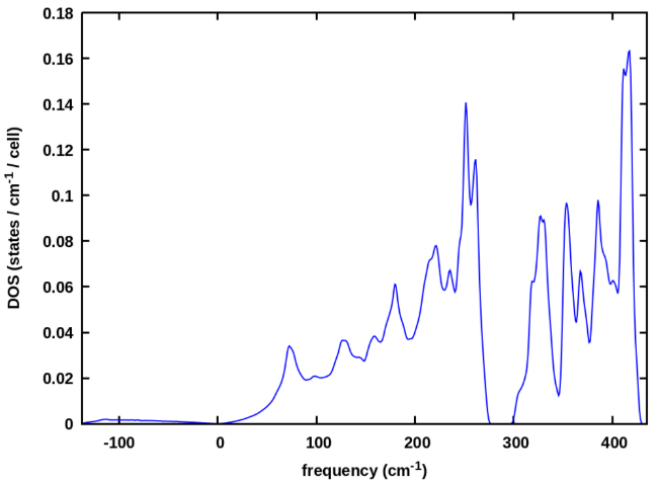

(b)

Figure 7. (a) Phonon dispersion curve and (b) Phonon DOS of LiFeP

6. SUPERCONDUCTING PROPERTIES

6.1. Electron-Phonon interaction

The electron-phonon interaction is essential to comprehend the superconducting phenomenon in the materials. The creation of electron-Cooper pairs is a key aspect of superconductivity, as is known from the Bardeen-Cooper-Schrieffer (BCS) hypothesis [40]. The interaction between electrons and phonons is the main factor that drives the creation of

Cooper pairs. At high temperatures, electrical and thermal resistance are dominated by the electron-phonon interaction. However, at low temperatures, the electron-phonon interaction produces electron pairs and forms an attractive interface, leading to superconductivity. The BCS theory states that the electron-phonon coupling is suitable only for weak coupling limitations. An understanding of many body processes led to the development of a sound theory [40–44].

Several superconducting properties are predicted using the Eliashberg theory [43], which allows the framework of the BCS theory for strong coupling constraints [44]. The current work uses density functional perturbation theory (DFPT) to determine the electron-phonon coupling (EPC) coefficient (λ). The primary source of data for the EPC constant (λ) is the Eliashberg spectral function $\alpha^2F(\omega)$, which is given as [43].

$$\alpha^2F(\omega) = \frac{1}{2\pi N(\varepsilon_F)}\sum_{qv}\frac{\Upsilon_{qv}}{\omega_{qv}}\delta\left(\omega - \omega_{qv}\right). \quad (1)$$

Where, the mathematical expression of Υ_{qv} is given in the reference [43].

The EPC coefficient (λ) is narrated as [45],

$$\lambda = 2\int\frac{d\omega}{\omega}\alpha^2F(\omega). \quad (2)$$

An exact definition of the superconducting transition temperature is given by McMillan's formula [42] as,

$$T_C = \frac{\theta_D}{1.45}\ exp\left[\frac{-1.04(1+\lambda)}{\lambda-\mu^*(1+0.62\lambda)}\right]. \quad (3)$$

In this case, μ^* stands for the static Coulomb pseudopotential. In the present work, μ^* is taken to be 0.1 [46]. Additionally, [47] provides the Debye temperature θ_D.

$$\theta_D = \frac{\hbar v_m}{k_B}, \quad (4)$$

where, $\hbar$ is the reduced Planck constant, v_m the Debye frequency and k_B the Boltzmann's constant, respectively.

The isotope effect exponent (α) is given in [48] as,

$$\alpha = \frac{1}{2}\left[1 - \left(\mu^*\, ln\frac{\theta_D}{1.45T_C}\right)^2\frac{1+0.62\lambda}{1.04(1+\lambda)}\right] \quad (5)$$

and, the effective interaction strength (N_0V) can be written as [48],

$$N_0V = \frac{\lambda-\mu^*}{1+10\lambda/11}. \quad (6)$$

Table 2 shows the values of λ, T_C, α and N_0V varying with the broadening of the Eliashberg spectral function $\alpha^2F(\omega)$ for studied materials.

Table 2. The superconducting parameters for LiFeP.

Broadening of $\alpha^2F(\omega)$	$\boldsymbol{\lambda}$	$\boldsymbol{T_C}$ (K)	$\boldsymbol{\alpha}$	$\boldsymbol{N_0V}$
0.005	0.2632	0.0325	0.3013	0.1317
0.010	0.2861	0.0689	0.3355	0.1477
0.015	0.2338	0.0041	0.2074	0.1103
0.020	0.1932	0.0000	0.0016	0.0793
0.025	0.1822	0.0000	-0.0920	0.0705
0.030	0.1880	0.0000	-0.0381	0.0752
0.035	0.2007	0.0001	0.0554	0.0852
0.040	0.2167	0.0010	0.1419	0.0975
0.045	0.2345	0.0046	0.2121	0.1109
0.050	0.2527	0.0148	0.2659	0.1242

Figure 8 displays the Eliashberg spectral function ($\alpha^2F(\omega)$) as a function of frequency ω. In most locations, where electron scattering has less of an impact, the shape of the spectral function ($\alpha^2F(\omega)$) is seen to be comparable to the phonon DOS (see **Figure 7(b)**). Here, Table 2 shows the values of λ, T_C, α and N_0V varying with the broadening, for LiFeP. Reciprocal variations of the isotope effect exponent α with T_C from **Table 2** are utilized to generate the isotope effect for the aforementioned superconductor and produce the superconducting behaviour. With the aid of α values, research is also being conducted on the impact of ionic vibration on the superconductivity of the material indicated above. It is found that the values of N_0V depend on the parameter λ. The weak coupling properties of the LiFeP superconductor can be quickly understood by estimating the fragile interaction strength from the values of N_0V [49]. It is cleared from comparing the values of λ and T_C that the maximum T_C is measured to be 0.0689K at the peak value of λ = 0.2861. The calculated value of T_C is substantially very lower than the experimental value of 6K [2]. Therefore, to reproduce the experimental value of T_C, the electron-phonon coupling needs to be taken 2.5-3.0 times stronger.

There is a difference between theoretical predictions and practical data, as the computed value of Tc is much lower than the experimentally observed value of 6 K [2]. The reason for this discrepancy is likely to be the limitations of traditional theories like BCS or Eliashberg,

which assume weak to moderate electron-phonon coupling. It is necessary to artificially increase the electron-phonon coupling strength by a factor of around 2.5 to 3.0 in order to reconcile this discrepancy and faithfully replicate the experimental value of T_C. The material may show stronger coupling behaviour or other mechanisms leading to superconductivity beyond those previously considered, as this adjustment makes up for the missing interactions or many-body effects not included in the original model. The materials under investigation, particularly those with complex interactions or unconventional superconductivity, have been found to have negative values for the isotope effect exponent. This suggests that increasing the atomic mass of a constituent element raises T_C, which is not the usual expectation. Strong electron-phonon coupling, polaronic effects, competing interactions, nonadiabatic or multi-band effects, complex substitution effects, and anharmonic effects are some of the possible explanations. Unlike iso-electronic LiFeAs, LiFeP, an iron-based superconductor, has nodal superconductivity. Strong spin fluctuations, weaker electronic correlations, and orbital competition are the causes of this disparity. Together, these components lower N_0V, which lowers Tc and is consistent with the lower T_C seen in LiFeAs [50].

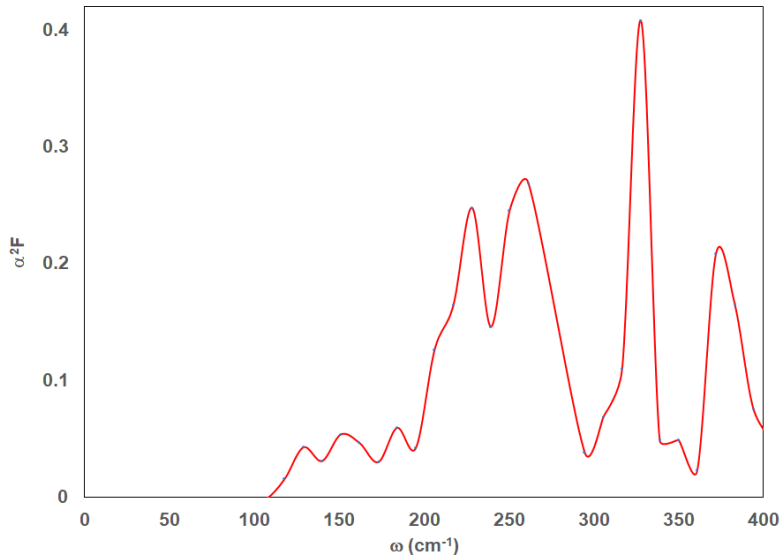

Figure 8. The spectral function $\alpha^2F(\omega)$ as a function of frequency ω

In iron-based superconductors like LiFeP, where conventional mechanisms (like BCS electron-phonon coupling) do not fully explain superconductivity, the claim that electron-phonon coupling is both weak and strong in LiFeP is in fact significant. However, electron-phonon interactions still play a significant role in these superconductors [51]. LiFeP is an intriguing illustration of a nodal, multiband superconductor that defies simple categorisation. Its extraordinarily large C/Tc ratio highlights the richness of its pairing process and provides

a rigorous test for any theoretical model of superconductivity in iron pnictides. Consequently, it remains a crucial element in the study of unconventional superconductivity [52, 53]. Generally, LiFeP - superconductor exhibits unconventional superconductivity with a nodal gap structure and no long-range magnetic order at ambient pressure. Its behaviour under applied pressure provides insight into the role of lattice, electronic, and magnetic degrees of freedom in shaping superconductivity. LiFeP becomes superconducting at a temperature of approximately 6K under ambient conditions, with line nodes believed to exist. Applied pressure suppresses the superconducting transition temperature, dropping from approximately 6 K at ambient pressure to around 3 K at around 2 GPa. LiFeP does not develop antiferromagnetic order, unlike many iron pnictides. High-pressure X-ray diffraction and transport studies show no evidence of a structural phase transition up to several GPa. The gap structure remains nodal under pressure, with no magnetic or structural transitions observed up to at least 2.5 GPa [52, 53].

7. CONCLUSIONS

The structural, electronic, vibrational, and superconducting properties of LiFeP superconductors were thoroughly examined in the present work using the generalized gradient approximation (GGA) method with ultrasoft pseudopotentials within the framework of the density functional theory (DFT) formalism. The calculated electronic band structure shows that the Fe 3d states play a dominant role in conduction because they are prominently located close to the Fermi level. The P 3s states are primarily located deep below the Fermi level, whereas the Li 3d states are found above it. The metallic nature of LiFeP is further supported by the existence of several bands that cross the Fermi level. Here, phonon dispersion analysis shows only positive phonon frequencies across the Brillouin zone and validates the dynamical stability of the optimised crystal structure. However, the superconducting transition temperature Tc calculated under the assumption of weak electron-phonon coupling significantly underestimates the experimentally reported value of approximately 6 K. This discrepancy suggests that the actual electron-phonon interaction may be significantly stronger than expected; an enhancement factor of 2.5 to 3.0 is most likely required to reconcile theoretical and experimental results. Furthermore, the low values of the effective interaction strength N_0V support the notion of weak electron-phonon coupling in the material, which is consistent with the modest superconducting transition temperature of LiFeP.

Acknowledgements

The Department of Science and Technology, Government of India, New Delhi, India, for building the computing facility under the DST-FIST programme, and the University Grants Commission, New Delhi, India, for financial support under the DRS-SAP-II programme, are both acknowledged by the author.

References

[1] Akande, S. O.: Calculations of Phonons and Phonon Dispersion in LiFeP Pnictide Superconductor. M. Sc. Thesis, African Univ. Sci. Tech. Abuja (2010). (https://repository.aust.edu.ng/xmlui/bitstream/handle/123456789/255/SALAWU%20OMOTAYO%20AKANDE.pdf?sequence=1&isAllowed=y)

[2] Dai, P., Hu, J., Dagotto, E.: Magnetism and its microscopic origin in iron-based high-temperature superconductors. Nature Phys. 8, 709-718 (2012). (DOI: https://doi.org/10.1038/nphys2438)

[3] Mitsen K. V., Ivanenko O. M. Cluster structure of superconducting phase and the nature of peaks in the doping dependences of the London penetration depth in iron pnictides. Res. Phys. 32, 105156 (2022). (DOI: https://doi.org/10.1016/j.rinp.2021.105156)

[4] Hosono H.: Iron Pnictide Superconductors: Discovery and Current Status. Mater. Matt. 4, 1-11 (2011). (https://www.sigmaaldrich.com/IN/en/technical-documents/technical-article/materials-science-and-engineering/batteries-supercapacitors-and-fuel-cells/iron-pnictide-superconductors)

[5] Zala V. B., Vora A. M., Gajjar P. N.: Electronic properties of iron pnictide superconductor LiFeP AIP Conf. Proc. 2100, 020027 (2019). (DOI: https://doi.org/10.1063/1.5098581)

[6] Shein I. R., Ivanovskii A. L: Electronic properties of novel 6 K superconductor LiFeP in comparision with LiFeAs from first principles calculations, Solid State Commun. 150, 152-156 (2010). (DOI: https://doi.org/10.1016/j.ssc.2009.10.021)

[7] Pešić, Jelena R.: Investigation of Superconductivity in Graphene and Related Materials Using Ab-Initio Methods. University of Belgrade, Serbia (2024). (https://www.proquest.com/docview/3073201082?sourcetype=Dissertations%20&%20Theses)

[8] Jonas Bekaert: Ab initio description of multicomponent superconductivity in bulk to atomically thin materials. Ph.D. Thesis, Department of Physics, Universiteit Antwerpen, Antwerpen (2018). (https://repository.uantwerpen.be/docman/irua/bcdaa4/151304.pdf)

[9] Kulkarni Shrikaant, Srivastava Vipul, William P.: Contemporary Advancements in Materials Technology-Novel Solutions to Complex Problems. Apple Academic Press, Florida (2025) (ISBN: 9781003561859)

[10] Cardwell David A., Larbalestier David C., Aleksander Braginski.: Handbook of Superconductivity - Fundamentals and Materials. Volume One, CRC Press, Florida (2022) (ISBN : 9780429179181)

[11] Johnson Peter D., Xu Guangyong, Yin Wei-Guo (Editors) : Iron-Based Superconductivity, Springer Series in Materials Science, Springer International Publishing, Switzerland (2015). (ISSN : 0933-033X)

[12] Ding Yimin, Xue Kui, Zhang Jing, Yan Luo, Li Qiaoqiao, Yao Yisen, Zhou Liujiang : Two-Dimensional Octuple-Atomic-Layer $M_2Si_2N_4$ (M = Al, Ga and In) with Long Carrier Lifetime, Micromachines. 14, 405 (2023). (DOI: https://doi.org/10.3390/mi14020405)

[13] Romanin Davide: Electron-phonon interactions in low-dimensional carbon systems: superconductivity and charge-density waves. Doctoral Dissertation, Graduate School of Politecnico di Torino, ScuDo, (2021). (https://iris.polito.it/retrieve/e384c433-060b-d4b2-e053-9f05fe0a1d67/Thesis_Romanin.pdf)

[14] Talantsev Evgueni F.: Quantifying Nonadiabaticity in Major Families of Superconductors. Nanomaterials 13, 71 (2023). https://doi.org/10.3390/nano13010071

[15] Kanoun Mohammed Benali, Goumri-Said Souraya: Theoretical Prediction of Electronic Structures and Phonon Dispersion of Ce_2XN_2 (X = S, Se, and Te) Ternary, Computation. 5, 29 (2017). (DOI :10.3390/computation5020029)

[16] Tapp J. H., Tang Z., Lv B., Sasmal K., Lorenz B., Chu P., Guloy A.: LiFeAs: An intrinsic FeAs-based superconductor with Tc=18 K. Phys. Rev. B78, 060505 (2008). (DOI: https://doi.org/10.1103/PhysRevB.78.060505)

[17] Kamihara, Y., Watanabe, T., Hirano. M., Hosono, H.: Iron-Based Layered Superconductor La[O1-xFx]FeAs (x = 0.05−0.12) with Tc = 26 K. J. Am. Chem. Soc. 130, 3296-3297 (2008). (DOI: https://doi.org/10.1021/ja800073m)

[18] Patel H. S., Dabhi V. A., Vora A. M.: Investigating Electronic, Optical, Thermodynamic, and Thermoelectric Properties of SrO and SrO2 Phases: A Density

Functional Theory Approach. ACS Omega 8, 43008 (2023). (DOI: https://doi.org/10.1021/acsomega.3c06221)

[19] Patel H. S., Dabhi V. A., Vora A. M.: First Principles Investigation of Electronic and Elastic Properties of Strontium Oxide and Strontium Peroxide Phases: Insights into Structural Stability and Phase Transitions. Physica Scripta 98, 125930 (2023). (DOI: 10.1088/1402-4896/ad0802)

[20] Vora Aditya M. : Study on Electronic Properties of α-Uranium using Ab-initio Approach. BIBECHANA 19, 208 (2022) (DOI : https://doi.org/10.3126/bibechana.v19i1-2.46838)

[21] Dabhi V. A., Patel H. S., Vora A.M.: Ab-initio Calculations of Structural, Vibrational, Electronic and Elastic Properties of Fluorite Minerals: A Computer Simulation Approach. Chinese Journal of Physics 89, 1266 (2024) (DOI : https://doi.org/10.1016/j.cjph.2024.01.015)

[22] Parmar Vandana B., Vora Aditya M. : Study of structural and electronic properties of $MnTiS_2$ compound. Sri Lankan Journal of Physics 23, 16 (2022) (DOI: http://doi.org/10.4038/sljp.v23i1.8098)

[23] Giannozzi P., Baroni S., Bonini N., Calandra M., Car R., Cavazzoni C., Ceresoli D., Chiarotti G., Cococcioni M., Dabo I., Dal Corso A.: QUANTUM ESPRESSO: a modular and open-source software project for quantum simulations of materials. J. Phys. Condens. Matte, 21, 395502 (2009). (DOI : 10.1088/0953-8984/21/39/395502)

[24] Perdew J. P., Burke K. Ernzerhof M.: Generalized Gradient Approximation Made Simple. Phys. Rev. Lett. 77, 386568 (1996). (DOI: https://doi.org/10.1103/PhysRevLett.77.3865)

[25] Vanderbilt D.: Soft self-consistent pseudopotentials in a generalized eigenvalue formalism. Phys. Rev. B41, 7892-7895 (1990). (DOI: https://doi.org/10.1103/PhysRevB.41.7892)

[26] Blöchl P. E., Jepsen O., Andersen O. K.: Improved tetrahedron method for Brillouin-zone integrations Phys. Rev. B49, 16223-16233 (1994). (DOI: https://doi.org/10.1103/PhysRevB.49.16223)

[27] Setyawan W., Curtarolo S.: High-throughput electronic band structure calculations: Challenges and tools. Comput. Mater. Sci. 49, 299-312 (2010). (DOI: https://doi.org/10.1016/j.commatsci.2010.05.010)

[28] Janert P. K.: Gnuplot in action : understanding data with graphs. (http://hadron.physics.fsu.edu/~eugenio/comphy/gnuplotbook.pdf)

[29] Monkhorst H. J., Pack J. D. Special points for Brillouin-zone integrations. Phys. Rev. B13, 5188-92 (1976) (DOI: https://doi.org/10.1103/PhysRevB.13.5188)

[30] Animalu A.: Intermediate Quantum Theory of Crystalline Solids, Prentice-Hall India Pvt. Ltd. (1978). (ISBN : 9780134707990)

[31] Kokalj A.: XCrySDen—a new program for displaying crystalline structures and electron densities J. Mol. Graph. Model. 17, 176-179 (1999). (DOI: https://doi.org/10.1016/S1093-3263(99)00028-5Get rights and content)

[32] Sadovskii, M. V.: High-temperature superconductivity in iron-based layered iron compounds. Phys. Uspekhi 51, 1201-27 (2008) (DOI: https://doi.org/10.1070/PU2008v051n12ABEH006820)

[33] Ivanovskii, A. L. : New high-temperature superconductors based on rare-earth and transition metal oxyarsenides and related phases: synthesis, properties and simulations. Physics-Uspekhi 51, 1229 (2008). (DOI: https://doi.org/10.1070/PU2008v051n12ABEH006703 VI)

[34] Izyumov, Y. A., Kurmaev, E. Z.: FeAs systems: a new class of high-temperature superconductors. Physics-Uspekhi, 51, 1261 (2008). (DOI : https://doi.org/10.1070/PU2008v051n12ABEH006733)

[35] Sadovskii, M. V. : High-temperature superconductivity in iron-based layered iron compounds. Physics-Uspekhi, 51, 1201 (2008). (DOI: https://doi.org/10.1070/PU2008v051n12ABEH006820)

[36] Singh, D. J., Du M. H.: Density Functional Study of $LaFeAsO_{1-x}F_x$: A Low Carrier Density Superconductor Near Itinerant Magnetism. Phys. Rev. Lett., 100, 237003 (2008). (DOI: https://doi.org/10.1103/PhysRevLett.100.237003)

[37] Subedi, A., Zhang L., Singh D. J. Du M. H.: Density functional study of FeS, FeSe, and FeTe: Electronic structure, magnetism, phonons, and superconductivity. Phys. Rev. B 78, 134514 (2008). (DOI: https://doi.org/10.1103/PhysRevB.78.134514)

[38] Mazin, I. I., Sigh D. J., Johannes M. D., Du M. H.: Unconventional Superconductivity with a Sign Reversal in the Order Parameter of $LaFeAsO_{1-x}F_x$. Phys. Rev. Lett., 101, 057003 (2008). (DOI: https://doi.org/10.1103/PhysRevLett.101.057003)

[39] Putzke, C., Clodea A. I., Guillamon I., Vif=gnolles D., McCollam A., Leboeuf D., Watson M. D., Mazin I. I., Kasahara S., Terashima T., Shibauchi T., Matsuda Y., Carrington A.: de Haas–van Alphen Study of the Fermi Surfaces of Superconducting

LiFeP and LiFeAs. Phys. Rev. Lett., 108, 047002 (2012). (DOI: https://doi.org/10.1103/PhysRevLett.108.047002)

[40] Hashimoto, K., Kasahara S., Katsumata R., Mizukami Y., Yamashita M., Ikeda H., Terashima T., Carrington A., Matsuda Y., Shibauchi T.: Nodal versus Nodeless Behaviors of the Order Parameters of LiFeP and LiFeAs Superconductors from Magnetic Penetration-Depth Measurements. Phys. Rev. Lett., 108, 047003 (2012). (DOI: https://doi.org/10.1103/PhysRevLett.108.047003)

[41] Allen P. B., Mitrovic B.: Theory of Superconducting Tc. Solid State Phys. 37, 1-92 (1982). (DOI: https://doi.org/10.1016/S0081-1947(08)60665-7)

[42] Carbotte J. P.: Properties of boson-exchange superconductors. Rev. Mod. Phys., 62, 1027-1157 (1990). (DOI: https://doi.org/10.1103/RevModPhys.62.1027)

[43] Eliashberg G. M.: Interactions Between Electrons and Lattice Vibrations in a Superconductor. JETP 11, 696–702 (1960). (http://www.jetp.ras.ru/cgi-bin/dn/e_011_03_0696.pdf)

[44] Sarasov S. Y., Sarasov D. Y.: Electron-phonon interactions and related physical properties of metals from linear-response theory. Phys. Rev. B54, 16487-16501 (1996). (DOI: https://doi.org/10.1103/PhysRevB.54.16487)

[45] Heid R.: Electron-Phonon Coupling: The Physics of Correlated Insulators, Metals, and Superconductors Modelling and Simulation Forschungszentrum Jülich GmbH (2017). (ISSN: 2192-8525)

[46] McMillan W. L.: Transition Temperature of Strong-Coupled Superconductors. Phys. Rev. 167, 331-344 (1968). (DOI: https://doi.org/10.1103/PhysRev.167.331)

[47] Kittel C.: Introduction to Solid State Physics, 8th Ed., John Wiley and Sons Inc. (2005) (ISBN: 0-471-41526-X)

[48] Vora A. M., Gandhi A. L. Theoretical Investigation of Superconducting State Parameters of Some Bulk Metallic Glasses using Pseudopotential Approach. J. Supercond. Nov. Magn. 33, 323-330 (2020). (DOI: https://doi.org/10.1007/s10948-019-05208-3)

[49] Pallikara I., Kayastha P., Skelton J. M., Whalley L. D.: The physical significance of imaginary phonon modes in crystals. Electron. Struct. 4, 033002 (2022). (https://doi.org/10.1088/2516-1075/ac78b3)

[50] Imai T., Ahilan K., Ning F. L., McQueen T. M., Cava R. J.: Why Does Undoped FeSe Become a High-Tc Superconductor under Pressure?. Phys. Rev. Lett. 102, 177005 (2009). (DOI: https://doi.org/10.1103/PhysRevLett.102.177005)

[51] Marsiglio F., Carbotte J. P.: Electron - Phonon Superconductivity, In: Bennemann, K.H., Ketterson, J.B. (eds) Superconductivity. Springer, Berlin, Heidelberg (2008). (DOI: https://doi.org/10.1007/978-3-540-73253-2_3)

[52] Hashimoto K., Kasahara S., Katsumata R., Mizukami Y., Yamashita M., Ikeda H., Terashima T., Carrington A., Matsuda Y., Shibauchi T.: Nodal versus Nodeless Behaviors of the Order Parameters of LiFeP and LiFeAs Superconductors from Magnetic Penetration-Depth Measurements. Phys. Rev. Lett. 108, 047003 (2012). (DOI: https://doi.org/10.1103/PhysRevLett.108.047003)

[53] Kim J. S., E. G. Kim1, Stewart G. R., Chen X. H., Wang X. F.: Specific heat in KFe2As2 in zero and applied magnetic field. Phys. Rev. B 83, 172502 (2011). (DOI: https://doi.org/10.1103/PhysRevB.83.172502)